Manuscript Details

Manuscript number	PRE_2019_715
Title	Material removal efficiency improvement by orientation control of CMP pad surface asperities
Article type	Research Paper

Abstract

This paper presents a novel method of improving material removal efficiency in the chemical mechanical polishing (CMP) process by optimizing the surface asperity orientation with respect to polishing motion. Feret's diameter plays a key role in increasing the number of working abrasives. Based on Feret's diameter model, an optimization method is proposed for the conditioning motion of a diamond dresser against a CMP pad. The radial velocity component of the dresser on the CMP pad is maximized by considering its direction of motion based on kinematic motion simulation. In addition, the pad cut rate profile is optimized to be uniform. Analytical and experimental investigations show that the ratio of radial and tangential velocity components is improved, yielding a larger Feret's diameter and 15% increase in the material removal rate.

Keywords	polishing; dress; conditioning; surface asperity; feret's diameter; polishing pad
Taxonomy	Semiconductor Manufacturing, Engineering

Corresponding Author	Norikazu Suzuki
Order of Authors	Norikazu Suzuki, Hirotaka Misono, Eiji Shamoto, Yohei Hashimoto, Hozumi Yasuda, Yoshihiro Mochizuki

Suggested reviewers	The review was finished by JSPE. The review was finished by JSPE.

Submission Files Included in this PDF

File Name [File Type]

Cover letter.docx [Cover Letter]

highlights.docx [Highlights]

PE_manuscript_final.docx [Manuscript File]

To view all the submission files, including those not included in the PDF, click on the manuscript title on your EVISE Homepage, then click 'Download zip file'.

Dear Editors-in-Chief,

This manuscript has been reviewed and accepted for publication on behalf of JSPE with No.JJSPE-D-19-00127.
I request Prof. Masanori Kunieda
as the Editor-in-Chief to be assigned.

Date of submission : 2019-07-11
Finished date of revision : 2019-10-22
Date of acceptance : 2019-10-31
(2019-11-02)

Best Regards,

Norikazu Suzuki

- A novel method of improving material removal efficiency in the chemical mechanical polishing (CMP) process by optimizing the surface asperity orientation with respect to polishing motion is presented.
- Based on Feret's diameter model, an optimization method is proposed for the conditioning motion of a diamond dresser against a CMP pad.
- The radial velocity component of the dresser on the CMP pad is maximized by considering its direction of motion based on kinematic motion simulation.
- Analytical and experimental investigations show that the ratio of radial and tangential velocity components is improved, yielding a larger Feret's diameter and 15% increase in the material removal rate.

Title: Material removal efficiency improvement by orientation control of CMP pad surface asperities

Authors: Norikazu Suzuki, Hirotaka Misono, Eiji Shamoto, Yohei Hashimoto, Hozumi Yasuda, Yoshihiro. Mochizuki

Affiliations: Nagoya University, Furo-cho, Chikusa-ku, Nagoya, Aichi, 464-8603, Japan

Department of Mechanical Engineering, Kanazawa University, Kanazawa, Ishikawa, Japan

Ebara Corporation, Fujisawa, Kanagawa, Japan

Abstract:

This paper presents a novel method of improving material removal efficiency in the chemical mechanical polishing (CMP) process by optimizing the surface asperity orientation with respect to polishing motion. Feret's diameter plays a key role in increasing the number of working abrasives. Based on Feret's diameter model, an optimization method is proposed for the conditioning motion of a diamond dresser against a CMP pad. The radial velocity component of the dresser on the CMP pad is maximized by considering its direction of motion based on kinematic motion simulation. In addition, the pad cut rate profile is optimized to be uniform. Analytical and experimental investigations show that the ratio of radial and tangential velocity components is improved, yielding a larger Feret's diameter and 15% increase in the material removal rate.

Keywords: Polishing; Dress; Conditioning; Surface asperity; Feret's diameter; Polishing pad

1. Introduction

In the 1990s, semiconductor industries introduced chemical mechanical polishing (CMP) to shallow trench isolation and interlevel dielectric planarization. Since then, there have been a wide range of CMP applications for device manufacturing [1]. With advances in modern semiconductor devices, CMP-based planarization performance has become increasingly important [2]. Defect-free planarization without scratch generation [3] and residual debris [4] is crucial for achieving high yield rates as well as precise control of within-wafer uniformity in material removal [5]. Manufacturing efficiency depends on two key factors. First, the material removal rate (MRR) must be maximized for a given cycle time. Second, the amount of CMP slurry, pad, and conditioner use must be minimized to improve cost efficiency. Hence, the current research focus is on the optimization of CMP process efficiency rather than only the MRR [6].

Fig. 1 shows schematic of the CMP process. The MRR is mainly governed by Preston's law, i.e., the MRR (MRR) is proportional to relative velocity v, polishing pressure p, and Preston's coefficient k, which represents polishing efficiency [7]. This well-known empirical model ($MRR = k \times p \times v$) shows that the MRR increases with Preston's coefficient, polishing load, and relative velocity. Relative velocity and polishing load are limited by the CMP machine configuration and process requirements. Preston's coefficient is affected by several process factors, particularly the functionality of the physical contact of abrasives and chemicals [8]. Materials are removed by the contact of nanoscale abrasives with chemically altered material surfaces. Hence, the material removal mechanics of nano-abrasives directly affect the efficiency of material removal. The surface asperities of polishing pads apply polishing force to actively working abrasives. Thus, the functionality of pad surface asperity is significant as well.

Cook developed a physical model for the contact between abrasives and glass workpieces to explain the material removal mechanism from a microscopic point of view. However, pad asperity contact was neglected [9]. Luo et al. proposed an extended model that considered pad asperity physical contact [10]. The model assumed that abrasives are trapped between an asperity–wafer interface, and thus, the MRR is approximately proportional to the asperity contact area, as shown in Fig. 1(b). Isobe et al. clarified that Feret's diameter of asperity contact significantly influences the MRR, where the MRR increases with Feret's diameter [11]. Pad surface asperities are generated through the conditioning of pads by dressers [12]. Based on Feret's diameter model shown in Fig. 1(c), Suzuki et al. explored a method of improving material removal efficiency through asperity geometry optimization, where the primary concept of increasing Feret's diameter by controlling dresser kinematic motion was presented [13]. Dresser kinematic motion is generally controlled to obtain a uniform pad cut rate (PCR) distribution over CMP pads [14]. PCR control is essential for achieving a stable CMP process in industry, as uneven CMP pad wear due to inappropriate dresser swing motion control deteriorates within-wafer nonuniformity [15].

Based on the past studies on Feret's diameter, a practical approach for improving material removal efficiency is proposed in the present study. The swing/rotational motion of a dresser and a pad is optimized, and asperity orientation is controlled to maximize Feret's diameter. In addition, the PCR distribution within a CMP pad is designed to maintain high uniformity. The influence of the proposed method on Feret's diameter and the MRR is experimentally investigated. Henceforth, the paper is organized as follows. Analysis of CMP pad surface asperity is explained in Section 2, followed by proposed asperity orientation

control approach to increase material removal efficiency in Section 3. Results of experimental verifications are presented in Section 4. The paper is concluded with a summary.

2. Analysis of CMP pad surface asperities

This section describes the analysis of asperity properties and the key factor that affects efficient material removal. Fig. 2 shows the height distribution of a polyurethane pad surface and the typical asperity measured by a laser microscope. The pad is IC1000™. It has been used in oxide CMP under typical polishing and dressing conditions. The asperity at the topmost position in the height direction comes in contact with a workpiece. As shown in Fig. 2, asperity geometry is observed in a hemiellipsoidal shape rather than a hemispherical shape. A series of investigations clarified that the ellipsoidal radii of asperities have a distribution. As the contact area of a hemiellipsoid against a flat wafer surface is elliptic, Feret's diameter varies depending on the relative motion direction, i.e., the polishing direction. For instance, when the relative motion direction is perpendicular to the major axis of the contact ellipse, Feret's diameter becomes the maximum on anisotropic contact geometry. Conversely, Feret's diameter is the minimum when the relative motion direction is perpendicular to the minor axis direction. Hence, the relative angle between the major axis of the contact ellipse and the relative motion direction is important.

It is well known that the relative polishing motion direction in the CMP process uniformly distributes on the wafer because the rotational speeds of the pad and wafer are almost the same in general. The relative polishing motion direction corresponds to the average tangential direction in the rotational motion of the polishing pad on the wafer. This suggests the importance of the relative angle between the asperity orientation direction and the tangential direction of pad rotation. Based on Feret's diameter, the geometrical features in contact asperities are analyzed by utilizing the primitive contact model proposed by Hashimoto et al. [16]. The asperities at the topmost position are extracted from the measured pad surface geometry, as shown in Fig. 2. Assuming a hemiellipsoid, the best fit geometry parameters, i.e., ellipsoidal radii and the orientation angle of the major radius direction, □, of the extracted asperity are identified using the least squares method. The nonlinear elastic deformation behavior of the identified ellipsoidal asperities is formulated by assuming Hertzian contact theory. The contact area of the asperities against the wafer is estimated under several nominal polishing pressure conditions. Feret's diameter of the estimated contact

geometry, $f(\theta)$, is calculated by assuming θ as the inclination angle of the relative motion direction to the tangential direction of pad rotation, as shown in Fig. 3.

Fig. 3 shows influence of θ on the total cumulative Feret's diameters of the contact ellipsoidal asperities, $\sum f(\theta)$, within a measured area of approximately 1.4 mm^2. The nominal compression pressure is assumed as 10 kPa to 30 kPa in the Hertzian contact simulation. The total Feret's diameter becomes the minimum around θ = 0°, as shown in Fig. 3. This indicates that the major axis tends to be oriented tangentially so that the average □ becomes zero. The average relative motion direction for wafer polishing is averagely identical to the tangential direction of pad rotation. Namely, θ is distributed around zero in the actual CMP process. The combination of the orientation angle (□ = 0°) and relative motion angle (θ = 0°) minimizes Feret's diameter. Thus, CMP is generally performed under the worst condition according to pad surface texture. In other words, the asperities are generally aligned to minimize material removal efficiency under the typical pad-conditioning procedure. Hence, material removal efficiency might be improved by modifying the asperity orientation direction based on the polishing direction.

3. Proposed asperity control approach to increase MRR

Experimental observations and the physics-based analyses described in the previous section indicate that the major direction of the elliptical asperity contact area tends to be oriented to the tangential direction of pad rotation. Suzuki et al. considered that this is caused by anisotropic pad conditioning motion [13]. Fig. 4 shows a typical CMP machine configuration and the schematic of pad conditioning. To prevent the deterioration of the pad surface due to polishing, the CMP pad is conditioned using a dresser, where diamond grains are generally fixed using a nickel plating technique. A dresser with a relatively small diameter is utilized in most device CMP processes to appropriately control the pad cut rate (PCR) profile along the radial direction of the pad, as shown in Fig. 4. The relative trajectory of the diamond abrasive is determined by the rotational motions of the dresser and pad and the swing motion of the dresser. The instantaneous relative motion vector, $\boldsymbol{v_{d-p}}(= v_{rad}\boldsymbol{e}_r + v_{tan}\boldsymbol{e}_t)$, consists of radial component v_{rad} and tangential component v_{tan}, where $\boldsymbol{e}_r$ and $\boldsymbol{e}_t$ are the unit radial and tangential vectors on the polishing pad, respectively. The diamond abrasive is considered to tear the topmost surface of the polyurethane pad into asperities with ellipsoidal geometry. Considering the cutting process with shear stress or tensile stress, the direction of the major radius of ellipsoidal asperities is likely to be along the relative motion of the diamond

abrasive against the polishing pad. It should be noted that asperity formation depends on other factors in addition to the conditioning direction. In particular, the pores inside polyurethane pads significantly influence asperity formation. The mechanism should be studied in more detail in future. However, the conditioning and asperity formation directions are considered to be stochastically correlated. This is also supported by the analyses described in Section 2. It should be noted that v_{tan} is dominant in the relative motion direction of pad conditioning; this is demonstrated in Section 4. In other words, Feret's diameter increases when the conditioning direction is controlled to be perpendicular to the polishing direction, as shown in Fig. 5. The polishing direction is almost the same the tangential direction of pad rotation, as mentioned earlier. Hence, conditioning motion should be perpendicular to the tangential direction. Namely, the radial component of the relative conditioning motion should be maximized for achieving better material removal efficiency.

The relative conditioning motion is simulated considering the rotation speeds of the dresser and polishing pad and the swing arm motion of the dresser. Fig. 6 illustrates the conditioning kinematics. The global position vector of point *P* can be calculated from the rigid body kinematics of the components, as follows:

$$\boldsymbol{r_p} = \boldsymbol{r_{sc}} + \boldsymbol{r_s} + \boldsymbol{r_d} \quad (1)$$

where $\boldsymbol{r_{sc}}$ and $\boldsymbol{r_s}$ are the relative position vectors of the swing and rotational centers, respectively, and $\boldsymbol{r_d}$ is the local position vector on the dresser contact surface. Diamond dresser velocity $\boldsymbol{v_d}$ is obtained from the angular velocity vectors of the dresser, $\boldsymbol{\omega_d}$, and the swing arm, $\boldsymbol{\omega_s}$, using Eq. (2).

$$\boldsymbol{v_d} = \boldsymbol{\omega_d} \times \boldsymbol{r_d} + \boldsymbol{\omega_s} \times \boldsymbol{r_s} \quad (2)$$

The pad rotational velocity is also calculated by utilizing the angular velocity vector of the pad, $\boldsymbol{\omega_p}$, using Eq. (3).

$$\boldsymbol{v_p} = \boldsymbol{\omega_p} \times \boldsymbol{r_p} \quad (3)$$

Then, the relative velocity for dressing is given by

$$\boldsymbol{v_{d-p}} = \boldsymbol{v_d} - \boldsymbol{v_p} \quad (4)$$

If Preston's law plays a dominant role in pad removal, the tangentially-averaged PCR, $M(r)$, can be formulated as a function of the radial position of the polishing pad, r, as given by Eq. (5).

$$M(r) = \frac{c_p}{2\pi T}\int_0^T\int_0^{2\pi}\sigma|\boldsymbol{v_{d-p}}|d\eta dt \quad (5)$$

where c_p is Preston's coefficient of pad removal, σ is conditioning pressure, η is an angle of the displacement vector, t is time, and T is a swing period. Considering the radial component, v_{rad} $(= \boldsymbol{v_{d-p}} \cdot \boldsymbol{e}_r)$, and the tangential component, $v_{tan}(= \boldsymbol{v_{d-p}} \cdot \boldsymbol{e}_t)$, of relative motion vector $\boldsymbol{v_{d-p}}$, the radial and tangential components of the tangentially-averaged PCR, $M(r)$, are formulated as follows:

$$M_{rad}(r) = \frac{c_p}{2\pi T}\int_0^T\int_0^{2\pi}\sigma v_{rad}d\eta dt \quad (6)$$

$$M_{tan}(r) = \frac{c_p}{2\pi T}\int_0^T\int_0^{2\pi}\sigma v_{tan}d\eta dt \quad (7)$$

Commercial CMP machines are commonly equipped with a swing speed control function, where swing arm angular speed $\omega_s = d\varphi/dt$ is controlled within the start and end angles (φ_{st} and φ_{en}). The angular range is divided into several zones. The angular speed for each zone is obtained by dividing angular range φ_i by stay time t_i, i.e., $\omega_i = \varphi_i/t_i$. The stay time for each zone is controlled arbitrarily to calibrate the PCR profile. The stay time is generally determined only to maintain high uniformity over the pad surface. In the proposed method, conventional uniformity control is performed along with the maximization of the ratio of M_{rad} to M_{tan}. Then, the radial velocity component of the relative motion of the diamond abrasive is maximized, resulting in a large Feret's diameter.

For the optimization of the rotation speeds and swing motion, the following objective function is postulated based on Eq. (8):

$$z = w_1\mathrm{std}(M(r)) + w_2\mathrm{mean}\left(\frac{M_{tan}(r)}{M_{rad}(r)}\right) \quad (8)$$

where $\mathrm{std}(M(r))$ is the standard deviation of $M(r)$, and $\mathrm{mean}\left(\frac{M_{tan}(r)}{M_{rad}(r)}\right)$ is the mean ratio of M_{rad} to M_{tan}. w_1 and w_2 are weight functions. Conditioning parameters can be optimized by minimizing the function consisting of PCR profile uniformity index $\mathrm{std}(M(r))$ and conditioning directional index $\mathrm{mean}\left(\frac{M_{tan}(r)}{M_{rad}(r)}\right)$. The weight functions are manually adjusted to obtain optimal solutions to balance both indexes. Fig. 7 illustrates the flow chart of the optimization procedure for conditioning parameters. The initial conditions for the PCR calculation are provided first. Then, the PCR profiles and objective functions are calculated using Eqs. (5)–(8). The downhill simplex method is applied, and the parameters for dressing conditions are optimized in a heuristic manner. Finally, the parameters that can simultaneously attain an even PCR profile and the large radial motion of the dresser are obtained.

4. Experimental verification

A series of experimental verifications were conducted by utilizing a commercial CMP machine equipped with an airbag type wafer carrier, as shown in Fig. 4. The angular speed of the dresser swing arm could be controlled independently in ten angular zones, which were evenly divided within the entire swing range. The IC1000™ single-layered polyurethane pads with concentric grooves were used. Two kinds of dressing conditions, i.e., optimal (Cond. 1) and worst (Cond. 2), were calculated and compared with the ordinary (Cond. 3) condition. In Cond. 2, $\mathrm{mean}\left(\frac{M_{rad}(r)}{M_{tan}(r)}\right)$ was minimized instead of $\mathrm{mean}\left(\frac{M_{tan}(r)}{M_{rad}(r)}\right)$ in Eq. (8). A constant dress stay time was applied in Cond. 3. Silicon wafers with thermal oxide films without patterns were polished by fumed silica based slurry, where ex-situ dress was applied. Before polishing wafers with the thermal oxide layer, pad break-in and glass dummy wafer marathon running were performed for the aging of the pad surface. In the aging step for each experiment, the total traveling distance of a single grain of the dresser on the CMP pad was set to be the same at approximately 25000 km. Namely, the total conditioning amounts before the MRR measurement tests were the same. Only relative motion directions were distributed differently. The dressing conditions are summarized in Table 1. Fig. 8 shows the profiles of input dress stay times for the designated zones and tangentially-averaged PCR profiles, where $c_p = 1$ is assumed. Fig. 9 shows the simulated trajectory of a diamond abrasive. Other conditions are summarized in Table 2.

As shown in Fig. 8, the simulated profiles of $M(r)$ are uniformly distributed within the wafer diameter, i.e., the PCR profiles are even, particularly in Cond. 1 and Cond. 2. As compared with Cond. 2 and Cond. 3, the mean ratio of radial and tangential components $(\frac{M_{tan}(r)}{M_{rad}(r)})$ in Cond. 1 becomes significantly small by utilizing the proposed optimization method. In contrast, $\frac{M_{tan}(r)}{M_{rad}(r)}$ is maximized in Cond. 2. The dress stay time profile was set to be constant without optimization in Cond. 3. Therefore, the evenness of the PCR profile is slightly deteriorated. The $\frac{M_{tan}(r)}{M_{rad}(r)}$ for Cond. 3 lies between those for Cond. 1 and Cond. 2. Fig. 9 visually demonstrates the trajectories of the single diamond abrasives on the polishing pad, where the features in radial motion of Cond 1, Cond. 2, and Cond. 3 are obviously different. The ratio of rotation speeds ω_p and ω_d strongly affects $\frac{M_{tan}(r)}{M_{rad}(r)}$. Hence, this ratio is quite important, and it has not been considered

in previous literature or in semiconductor industries. The simultaneous adjustment of the dress stay time and dresser rotation speed ratio can help in attaining a high MRR in practical use.

The experimental results of the MRR profile are shown in Fig. 10. The MRR in Cond. 1 is increased by approximately 15% compared with Cond. 3. The worst MRR is obtained in Cond. 2. The results of the MRR agree with the conditioning optimization results shown in Fig. 8(b). Even though the uniformity of the MRR is not good owing to center-fast profiles, the phenomena depend on not the proposed asperity orientation control but the characteristic of the CMP machine used for the experiment.

Fig. 11 shows measured three-dimensional profiles of the CMP pads after the experiments. Distinctive features in asperity orientation cannot be identified between Cond. 1, 2, and 3 through the visual observation of the measured profiles. The measured profiles are analyzed using a method similar to that described in Section 2, where the analysis focused on only the measured geometric profile without including the physics-based model. First, we find the height at which the total cross-sectional area of asperities becomes 1% of the nominal area. Then, each asperity cross section at this height is extracted, and Feret's diameter components f_t and f_r are calculated assuming that the relative motion direction is the same as the tangential and radial directions, respectively. For simplicity, the elastic deformation of asperity is not considered. The ratio, $\sum f_t / \sum f_r$, of the cumulative Feret's diameters in the total measured area is calculated. Note that a larger ratio should increase the effective Feret's diameter and thus material removal efficiency. Analytical investigations verified that the largest ratio of Feret's diameters in the radial and tangential directions is 1.097, which is observed from the polishing pad in Cond. 1. Ratios of 0.838 and 0.837 are observed in Cond. 2 and Cond. 3, respectively; these values are smaller compared with Cond. 1. As there is no difference between the ratios obtained in Cond. 2 and Cond. 3, the reliability of the analyses should be improved by increasing the number of evaluation samples in future research. However, the analytical results indirectly support the effectiveness of the proposed method. Namely, material removal efficiency is increased by optimizing the asperity orientation angle.

The proposed method can be applied to the CMP processes in industry by simultaneously modifying the recipes for swing arm motion control and the dresser/pad rotation speed ratio. The present research verified that the mean ratio, $\mathrm{mean}\left(\frac{M_{rad}(r)}{M_{tan}(r)}\right)$, can increase up to about 1, as listed in Table 1, but not more. This is because the dresser geometry and its rotational motion constrain the controllable range of the relative motion direction for pad conditioning. Hence, based on the proposed concept, further improvement may be

possible by the development of advanced CMP machines to perform selective dressing along the radial direction.

5. Conclusion

This study proposed a novel optimization approach to enhance material removal efficiency in the CMP process. It is clarified that the pad asperity shape plays a critical role by introducing a key directional relationship for optimizing pad dressing motion. The conclusions are summarized below.

1. Pad surface analysis revealed that asperities are typically shaped as ellipsoids, and the major axis direction of a contact ellipse tends to be oriented to the tangential direction of polishing pad rotation. Therefore, Feret's diameter is generally minimized and material removal efficiency becomes low.
2. The major radial axis of asperity is stochastically oriented towards the conditioning direction. Based on dressing simulation, pad dressing conditions are optimized by the proposed method. The radial component of the relative conditioning motion is maximized, yielding a large Feret's diameter and a high MRR.
3. Experimental investigations verified that the MRR can be increased up to 15% by simply tuning dressing motion kinematics such as dresser swing arm velocity and the pad/dresser rotation speed ratio.
4. The proposed method is simple, and it can be applied to modern CMP machines only by modifying dressing conditions. As a result, the method can be utilized for CMP process optimization to attain high material removal efficiency.

References:

[1] Saka N, Lai JY, Chun J-H, Shu NP (2001) Mechanisms of the chemical mechanical polishing (CMP) process in integrated circuit fabrication. CIRP Annals 50(1):233-238.

[2] Babu S (2016) Advances in Chemical Mechanical Planarization (CMP). Woodhead Publishing.

[3] Saka N, Eusner T, Chun J-H (2010) Scratching by pad asperities in chemical–mechanical polishing. CIRP Annals 59(1):329-332.

[4] Shin WK, An JH, Jeong HD (2011) Optimization of the physical cleaning condition for nanotechnology. CIRP Annals 60(1):579-582.

[5] Suzuki N, Hashimoto Y, Yasuda H, Yamaki S, Mochizuki Y (2017) Prediction of polishing pressure distribution in CMP process with airbag type wafer carrier. CIRP Annals 66(1):329-332.

[6] Wang P, Gao RX, Yan R (2017) A deep learning-based approach to material removal rate prediction in polishing. CIRP Annals 66(1):429-432.

[7] Preston FW (1927) The theory and design of plate glass polishing machines. J. Soc. Glass Technol. 11: 214-256.

[8] Wang C, Sherman P, Chandra A, Dornfeld D (2005) Pad surface roughness and slurry particle size distribution effects on material removal rate in chemical mechanical planarization. CIRP Annals 54(1):309-312.

[9] Cook LM (1990) Chemical processes in glass polishing. J. Non-Cryst. Solids 120(1-3):152-171.

[10] Luo J, Dornfeld DA (2001) Material removal mechanism in chemical mechanical polishing: theory and modelling. IEEE Trans. Semicond. Manuf. 14(2):112-133.

[11] Isobe A, Akaji M, Kurokawa S (2013) Proposal of new polishing mechanism based on Feret's diameter of contact area between polishing pad and wafer. Jap. J. Appl. Phys. 52:126503.

[12] Jeong HD, Park KH, Cho KK (2007) CMP pad break-in time reduction in silicon wafer polishing. CIRP Annals 56(1):357-360.

[13] Suzuki N, Oshika S, Misono H, Hashimoto Y, Yasuda H, Mochizuki Y (2017) Improvement of material removal efficiency by optimization of anisotropic contact of pad asperities. Proceedings of International Conference on Planarization/CMP Technology 95-99.

[14] Li ZC, Baisie AE, Zhang XH (2012) Diamond disc pad conditioning in chemical mechanical planarization (CMP): A surface element method to predict pad surface shape. Precis. Eng. 36(2):356-363.

[15] Lee H, Lee S (2017) Investigation of pad wear in CMP with swing-arm conditioning and uniformity of material removal. Precis. Eng. 49:85-91.

[16] Hashimoto Y, Oshika S, Suzuki N, Shamoto E (2015) A new contact model of pad surface asperities utilizing measured geometrical features. Proceedings of International Conference on Planarization/CMP Technology 46-49.

Figure / Table Captions

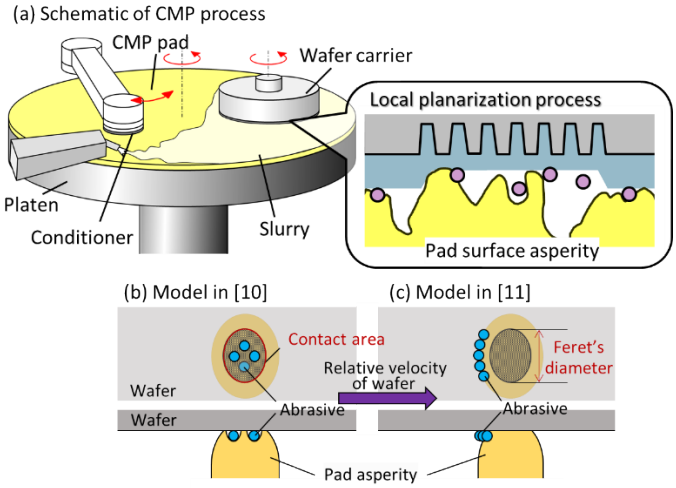

Fig. 1. Schematic of (a) general configuration of CMP process and (b) material removal models proposed in [10] and (c) [11].

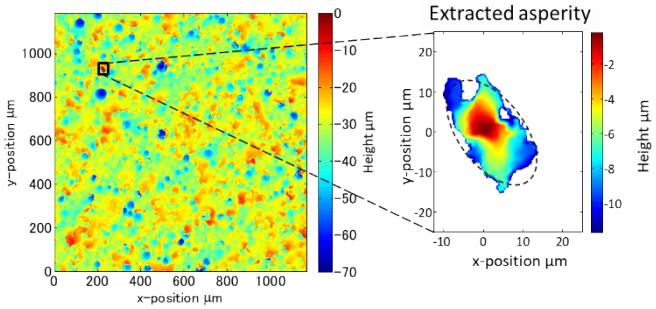

Fig. 2. Pad surface asperities measured by laser microscope.

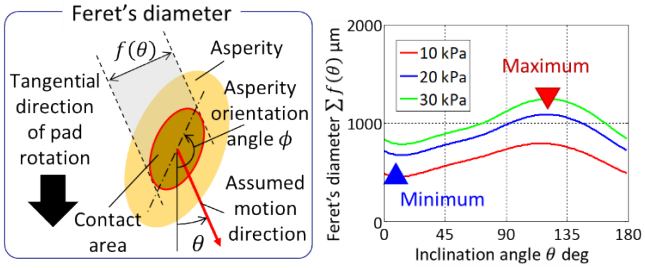

Fig. 3. Influence of inclination angle θ on Feret's diameter.

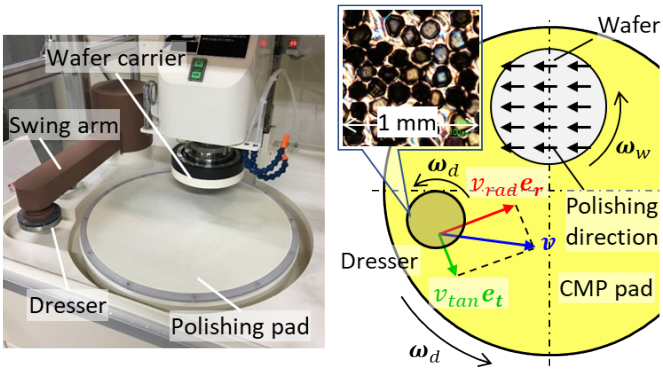

Fig. 4 CMP machine configuration with diamond dresser.

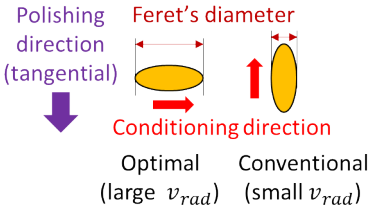

Fig. 5. Relative dressing direction to increase Feret's diameter.

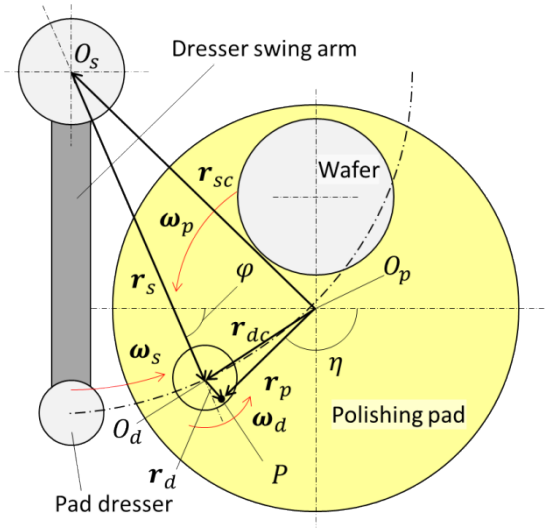

Fig. 6. Motion kinematics of dresser and polishing pad.

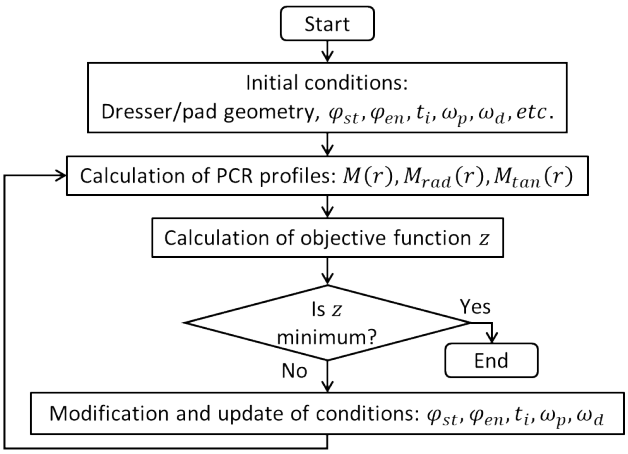

Fig. 7. Flow chart of dressing parameter optimization.

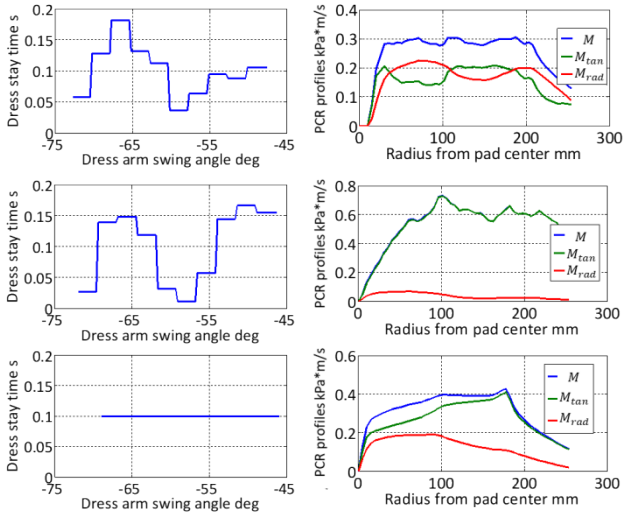

(a) input stay time profile (b) tangentially-averaged PCR profile

Fig. 8. Optimized dress stay time profiles and simulated PCR profiles. (Top: Cond. 1, Middle: Cond. 2, Bottom: Cond. 3)

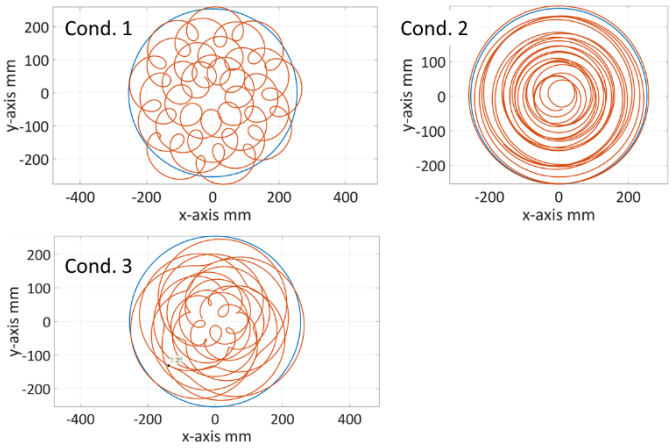

Fig. 9. Simulated trajectories of single diamond abrasive on polishing pad.

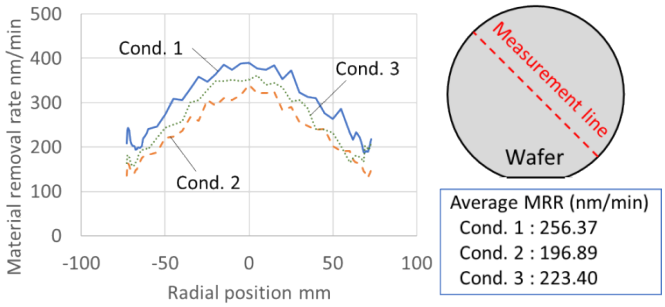

Fig. 10. Comparison of measured MRR profiles.

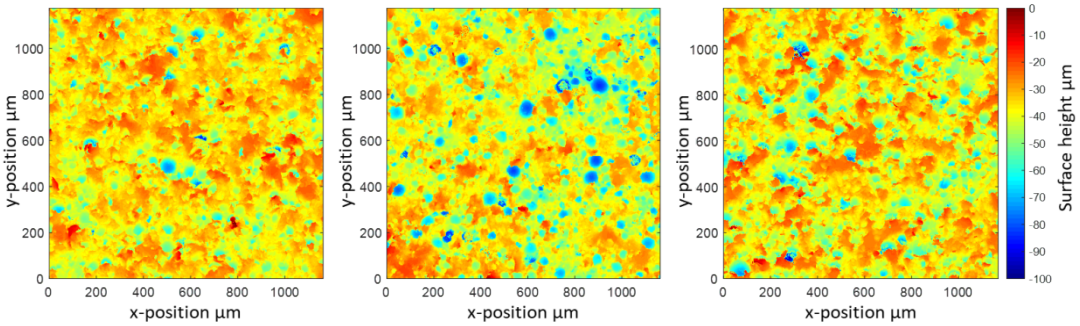

(a) Cond. 1 (b) Cond. 2 (c) Cond. 3

Fig. 11. Comparison of measured pad surface asperities.

Table 1: Dressing conditions and calculation results.

		Cond. 1	Cond. 2	Cond. 3
Dressing conditions	ω_p min^{-1}	23	138	70
	ω_d min^{-1}	200	30	114
	Stay time design	Optimal	Worst	Ordinary (Constant)
	Mean (M_{rad}/M_{tan})	1.11	0.04	0.31

Table 2: Experimental conditions.

Dressing conditions	Style		Ex-situ
	Load	N	58.8
	Diameter	mm	□100
	Grid number		#100
Polishing conditions	Pressure	kPa	20 (airbag with retainer ring)
	ω_w	min^{-1}	61
	ω_p	min^{-1}	60
	Slurry	ml/min	150 (KOH, ph11)
	Pad type		IC1000™
		mm	Φ508
	Wafer	mm	Φ150 (Thermal oxide)
	Polishing time	min	2